AIChE

Mass/Heat Transfer from a Neutrally Buoyant Sphere in Simple Shear Flow at Finite Reynolds and Peclet Numbers

Chao Yang
Key Laboratory of Green Process and Engineering, Institute of Process Engineering, Chinese Academy of Sciences, Beijing 100190, P.R. China

School of Chemical and Biomolecular Engineering, Cornell University, Ithaca, NY 14853

Jingsheng Zhang
Key Laboratory of Green Process and Engineering, Institute of Process Engineering, Chinese Academy of Sciences, Beijing 100190, P.R. China

Donald L. Koch
School of Chemical and Biomolecular Engineering, Cornell University, Ithaca, NY 14853

Xiaolong Yin
Dept. of Petroleum Engineering, Colorado School of Mines, Golden, CO 80402

DOI 10.1002/aic.12370
Published online August 17, 2010 in Wiley Online Library (wileyonlinelibrary.com).

Theoretical analyses of mass/heat transfer from a neutrally buoyant particle in simple shear flow indicate that mass/heat must diffuse across a region of closed streamlines of finite thickness at zero Reynolds number, whereas spiraling streamlines allow the formation of a thin mass transfer boundary layer at small but non-zero Reynolds numbers (Subramanian and Koch, Phys Rev Lett. 2006;96:134503; Subramanian and Koch, Phys Fluids. 2006;18: 073302). This article presents the first numerical results for mass/heat transfer at finite Reynolds and Peclet numbers. The simulations indicate that fluid particles in the flow-gradient plane spiral away from the particle for Reynolds numbers smaller than about 2.5 while they spiral toward the particle for higher Reynolds numbers. Solutions of the Navier-Stokes equations coupled with a boundary layer analysis of mass transfer yield predictions for the rate of mass transfer at asymptotically large Peclet numbers and Reynolds numbers up to 10. Simulations of mass transfer for zero Reynolds number and finite Peclet numbers confirm Acrivos' (Acrivos, J Fluid Mech. 1971;46:233–240) prediction that the Nusselt number approaches a finite value with increasing Peclet number. Simulations at finite Reynolds numbers and Peclet numbers up to 10,000 confirm the theoretical predictions for the concentration gradient at the particle surface at angular positions away from the flow-gradient plane. However, the wake near the flow-gradient plane remains too large at this Peclet number to yield a quantitative agreement of the overall rate of mass transfer with the theory for asymptotically large Peclet number. © 2010 American Institute of Chemical Engineers *AIChE J,* 57: 1419–1433, 2011

Keywords: shear flow, mass transfer, numerical simulation, boundary layer analysis, sphere

Introduction

Asymptotic analyses for small Reynolds numbers and high Peclet numbers[1,2] indicate that fluid inertia alters the topology of the fluid motion around a neutrally buoyant particle in a simple shear flow, greatly enhancing the rate of mass and heat transfer. At zero Reynolds number, a region of closed streamlines envelops the particle and scalar tracers must diffuse across this region to escape the particle. This leads to a Nusselt number that approaches a constant at high Peclet number.[3] At small but nonzero Reynolds numbers, Subramanian and Koch[1,2] showed that the streamlines in the flow-gradient plane spiral away from the particle allowing the formation of a thin boundary layer and a Nusselt number that grows indefinitely with increasing Peclet number. While these results are intriguing, they have been derived only in a dual asymptotic limit. The purpose of the present study is to use numerical solutions of the Navier-Stokes and advection-diffusion equations to extend our understanding of mass and heat transfer from neutrally buoyant spheres in shear flow to finite Reynolds and Peclet numbers.

Most previous studies on the mass/heat transfer from solid particles, drops, and bubbles have considered the fluid motion driven by a relative translation between the particle and surrounding fluid as would occur if the particle is settling in a quiescent fluid.[4–9] Such a flow involves open streamlines near the particle surface at all particle Reynolds numbers. At high Peclet numbers, the concentration disturbance due to a particle acting as a source of mass is confined to a thin boundary layer and a wake behind the sphere leading to a rapid rate of mass transfer. For example, Acrivos and Goddard[6] showed that the mass transfer rate at low Reynolds number is given by $Nu = 1.25\, Pe_U^{1/3} + 0.99$, where the Nusselt number is $Nu = ka/D$, the Peclet number based on the relative velocity U between the particle and fluid is $Pe_U = Ua/D$, the mass transfer coefficient is k, the diffusivity of the tracer is D, and the sphere radius is a. Numerical simulations confirm the $Pe_U^{1/3}$ scaling and show that it extends to finite Reynolds numbers. For zero Reynolds number and $10 < Pe_U < 2000$, the best fit to the simulations gives $Nu = 1.29\, Pe_U^{1/3} + 0.98$ close to the prediction from the boundary layer theory. Simulations have also incorporated transient effects, fluid–fluid interfaces and non-spherical particles.[5,10–12] Recently for example, Li et al.[10] used a finite-volume method with the SIMPLE algorithm to study the transport characteristics to or from spheroidal bubbles and solids immersed in a two-dimensional axisymmetric flow field and characterized the transfer rate as a function of Reynolds and Schmidt numbers and geometric parameters.

The fluid motion relative to a spherical particle can be dominated by shear when the density difference between the particle and fluid are small (e.g., biological cells), the shear rate is high and the particle size small (slurry reactors and microfluidic handling of colloids), or the fluid viscosity is high (emulsion polymerization). When the imposed flow is nearly unidirectional and the length scale of the macroscale flow is large compared with the particle size, then the local flow seen by the particle can be approximated as a simple shear flow. It is this situation that is the focus of the present article. The relevant Reynolds numbers Re and Peclet numbers Pe are those based on the shear rate of the fluid, i.e., $Re = \dot{\gamma} a^2/\nu$ and $Pe = \dot{\gamma} a^2/D$ (or $Pe = \dot{\gamma} a^2/\alpha$ for heat transfer). Here, $\dot{\gamma}$ is the velocity gradient of the imposed flow which is given in Cartesian coordinates by $\mathbf{u}^\infty = (\dot{\gamma} y, 0, 0)$, ν is the kinematic viscosity of the fluid, and α is the thermal diffusivity. We will consider the situation in which Re is in the range 0–10, while the Peclet number can be as large as 10,000. This implies that we require the Prandtl number $Pr = \nu/\alpha$ or Schmidt number $Sc = \nu/D$ to be large. The Prandtl number is large in highly viscous fluids whereas the Schmidt number is on the order of 10^4 even for small diffusing tracer molecules in aqueous solutions.

Batchelor[13] studied the rate of mass transfer from a neutrally buoyant particle in a three-dimensional linear flow field at $Re = 0$ to determine the mass transfer from sub-Kolmogorov particles in an isotropic turbulent flow. He argued that the rotation of the particle and fluid near the particle surface caused the particle to have a concentration field that was nearly independent of the azimuthal angle in a spherical coordinate system whose axis was aligned with the vorticity axis. In this way, he reduced the problem of mass transfer in a three-dimensional linear flow to that due to an axisymmetric extensional flow based on the extension rate along the vorticity axis. The open streamlines of this flow yield a thin boundary layer and a Nusselt number that grows in proportion to $Pe^{1/3}$ at high Peclet number. Batchelor's analysis, however, does not apply to two-dimensional linear flows including simple shear flow.

At zero Reynolds number, a neutrally buoyant particle in simple shear flow is surrounded by a region of closed streamlines. At high Peclet number, the concentration along each streamline is a constant but it is not equal to the concentration of the fluid far from the sphere. Acrivos[3] solved for the diffusive flux across streamlines and thereby found the rate of heat transfer for $Re = 0$ and $Pe \gg 1$ to be $Nu \approx 4.5$. The finite value of the Nusselt number in the limit of high Peclet number reflects the diffusive resistance of a region of closed streamlines of finite thickness. We will perform numerical simulations of mass transfer at $Re = 0$ and finite Pe and thereby observe the approach of the Nusselt number to this limiting value with increasing Pe.

Peery[14] performed a regular perturbation analysis to determine the first, $O(Re)$ effects of fluid inertia on the fluid velocity field around a sphere in simple shear flow. However, it was only 40 years later that Subramanian and Koch[2] showed that the broken symmetry resulting from the inertial velocity field made streamlines near the sphere become opening, instead of the closed configurations at $Re = 0$. For $Re \ll 1$ but $Re \neq 0$, centrifugal forces cause fluid particles

Correspondence concerning this article should be addressed to C. Yang at chaoyang@home.ipe.ac.cn.

in the flow-gradient plane to spiral away from the solid particle. The fluid flux required to compensate for this outward flow is drawn inward toward the sphere along the vorticity axis. A thin boundary layer is formed leading to an unbounded growth of the Nusselt number at high Peclet number, i.e., $Nu = (0.325 - 0.126\,Re^{1/2})\,(Re\,Pe)^{1/3} + O(1)$ for $Re \ll 1$ and $Pe\ Re \gg 1$. In the present article, we will extend this boundary layer analysis to finite Re. We will also assess the accuracy of the analysis at large but finite Pe.

Most previous numerical simulation studies of particles in shear flow have focused on the lift force or migration velocity resulting from the coupling of shear and particle rotation with a relative translation of the particle and fluid or a quadratic component of the flow.[15–19] However, Mikulencak and Morris[20] used a finite element method to simulate the fluid flow around a neutrally buoyant sphere in simple shear flow at finite Reynolds numbers and determined the particle's contribution to the stress and the particle rotation rate. Comparisons with this study will help to validate the present numerical solutions. Our calculations for the particle stresslet can also be compared with asymptotic analysis for small, but nonzero, Reynolds numbers (Subramanian et al., submitted; Stone et al., Personal communication).[21]

In this article, we use a finite volume numerical method to determine the fluid velocity and chemical tracer concentration fields around a neutrally buoyant particle in simple shear flow at finite values of the Reynolds and Peclet numbers. Section 2 describes the numerical methods. In Section 3, we present results for the fluid velocity field and the particle stresslet making comparisons with previous asymptotic and numerical analyses. In Section 4, the fluid velocity derivatives at the particle surface determined from the flow simulation are used as the basis of a boundary layer theory valid for $Pe \gg 1$ and $Re = 0(1)$. Finally, in Section 5, we present results of numerical solutions of the advection-diffusion equation for the tracer concentration field and the rate of mass transfer in Stokes flows as well as finite Reynolds number flows.

Scheme of Numerical Simulation

In this study, a finite difference method is adopted to solve the Navier-Stokes equations for the flow field around a torque-free neutrally buoyant sphere. The computational domain in a three-dimensional spherical coordinate system (r, θ, ϕ), whose origin is at the center of the sphere, is $a \le r \le R$, $0 \le \theta \le \pi$, and $0 \le \phi \le 2\pi$ for the two-phase flow and mass/heat transfer from a neutrally buoyant sphere at finite Reynolds number in simple shear flow, where R is the size of the outer boundary in the radial direction. All the governing equations of the flow and mass transfer are discretized on a staggered grid, which is uniform in the azimuthal (ϕ) and polar (θ) directions, but nonuniform in the radial (r) direction. In practice, 10–20 nodes of the grid near the sphere in the radial (r) direction are set to be tight and uniform since the velocity and the concentration vary more rapidly in this region, but after that an exponential relation, $r(n+1) = r(n)e^{n\alpha}$, is applied to determine the positions of nodes away from the sphere, where $r(n)$ denotes the nth node away from the sphere in the radial direction and α is a small constant that can be used to adjust the grid spacing.

For the computation of the fluid field around a neutrally buoyant sphere, the control volume formulation with the SIMPLE algorithm[22] is adopted to solve the shear flow at finite Reynolds number, and the velocities at $\theta = 0$ and π are taken to be azimuthal averages of second-order Adams-Bashforth extrapolations.[19] The effect of grid resolution on the predicted rotation rate and stresslet for a sphere at different Re was tested to ensure the accuracy of the results. One feature that makes this computation challenging even at small Re is that the outer boundary must be larger than the length scale $aRe^{-1/2}$ on which the inertial and viscous terms are comparable. While the first, $O(Re)$, correction to the fluid velocity field and stresslet and the $O(RePe)^{1/3}$ contribution to the Nusselt number result from a regular perturbation to the Stokes velocity field, the $O(Re^{3/2})$ contributions to the fluid velocity and stresslet and the $O(Re^{5/6}Pe^{1/3})$ contribution to the Nusselt number arise from terms in the inner region near the sphere driven by matching with the outer, inertial region. We have tested the grid refinement for nearly all calculated particle Reynolds numbers to ensure sufficient spatial computational accuracy. For example, under the condition that the smallest grid size in the radial direction, Δr, is $0.0025a$, we applied various nonuniform grids of $60(r) \times 30(\theta) \times 60(\phi)$ $(R = 10a)$, $80(r) \times 30(\theta) \times 60(\phi)$ $(R = 20a)$, $120(r) \times 30(\theta) \times 60(\phi)$ $(R = 90a)$, $140(r) \times 20(\theta) \times 40(\phi)$ $(R = 200a)$, $140(r) \times 30(\theta) \times 60(\phi)$ $(R = 200a)$, and $140(r) \times 40(\theta) \times 80(\phi)$ $(R = 200a)$ for calculating the rotation rate and hydrodynamic stresslet of a sphere in simple shear flow. We found that $R = 90a$ and a grid with $120(r) \times 30(\theta) \times 60(\phi)$ nodes suffice for Re as small at 10^{-3}. For larger particle Reynolds numbers, flows generally produce wakes that stretch to large distances in the streamwise direction, which will result in significant increase in the number of computing iterations required for achieving an acceptable level of convergence with increasing computing domain size,[20] or even makes the computation diverge if the computing domain size surpasses some values. Thus, it is necessary to limit the size of the outer boundary to avoid numerical instabilities. A Reynolds number that measures the importance of inertia on the length scale R is $Re(R/a)^2$, which takes on the value 4000 when $R = 20a$ and $Re = 10$.

In the study of mass transfer from a neutrally buoyant sphere in simple shear flow, we assume that the physical properties including mass diffusivity, fluid viscosity, and density are constant and not influenced by the concentration of solute, no solid–liquid interface resistance to mass transfer exists and the concentration at the solid–liquid interface is constant. Thus, the mass transfer does not affect the flow structure and the solution of the fluid flow and advection-diffusion equations is decoupled. The momentum transfer problem can be solved first and the resulting velocity field is utilized to formulate the time evolution of concentration field. In our simulation, the flow field and then the mass transfer are computed with the same grid resolution described above. The smallest dimensionless mesh size in the radial direction next to the particle surface is ensured less than $O(Pe^{-1/3})$, and we have also tested the grid refinement for the calculation of mass transfer to make sure the predicted mass transfer rates are independent of the mesh size. The grid resolution required for the mass transfer calculation is more stringent than that required for the flow field calculation. We

study situations where $Pe \gg 1$ so that the mass transfer boundary layer near the particle is thin and requires fine grid resolution. On the other hand, the maximum Reynolds number considered is 10 and this does not lead to a thin momentum boundary layer. Thus, a grid which is adequate for mass transfer will also be sufficient for the flow calculation.

The main calculation steps of this algorithm are outlined as follows: (1) initialize the flow field ($\mathbf{u}$ and P) with the sphere at rest, physical parameters (density, viscosity, and molecular diffusivity of solute), shear rate, and concentration; (2) compute the velocity, pressure, and rotation rate to steady state based on the torque-free rotation criterion using the SIMPLE algorithm and Newton's method[20]; (3) compute the concentration field in the fluid with the steady state flow field, and calculate the corresponding mass transfer rates and Nusselt numbers. Moreover, in Step 3, a fifth-order WENO (weighted essentially nonoscillatory) scheme in spatial discretization and a third-order TVD (total variation diminishing) Runge–Kutta scheme in time for the unsteady mass transfer are adopted for the solution of the advection-diffusion transport equation for sufficiently accurate results.[11] The transient calculation of mass transfer was assumed to have reached steady state if the change in the Nusselt number during that last 1/5 of the computational time was less than 1%.

Simple Shear Flow Around a Neutrally Buoyant Sphere

In this section, we present results of numerical simulations of the fluid flow around a neutrally buoyant particle in simple shear flow. We will examine the streamline pattern and fluid velocity field making comparisons with low Reynolds number analysis and pointing out an important change in streamline topology occurring at a critical Reynolds number. We also compare computational results for the rotation rate and particle stresslet with previous experimental, numerical, and analytical results.

A rigid force- and torque-free sphere is at the origin in a Newtonian fluid flow that is undergoing simple shearing motion far from the particle. The force-free condition is satisfied by a particle with zero translational velocity. The flow direction is denoted by x or 1, velocity gradient direction by y or 2, and vorticity direction by z or 3. The velocity $\mathbf{u}(\mathbf{r})$ and the pressure $p(\mathbf{r})$ in the fluid are governed by the continuity and steady momentum conservation equations in dimensionless forms:

$$\nabla \cdot \mathbf{u} = 0 \tag{1}$$

$$\mathbf{u} \cdot \nabla \mathbf{u} = -\nabla p + \frac{1}{Re}\nabla^2 \mathbf{u} \tag{2}$$

Lengths are non-dimensionalized by the sphere radius a, velocities by $a\dot{\gamma}$, and stresses by $\mu\dot{\gamma}$, where $\dot{\gamma}$ is the velocity gradient of simple shear flow and μ is the dynamic viscosity of the fluid. The fluid velocity on the surface of the sphere is $\mathbf{u} = \Omega \times \mathbf{r}$ according to the no-slip boundary condition, where $\Omega = \varpi \mathbf{e}_z$ is the rotation rate of the sphere under the condition of no hydrodynamic torque, i.e.,

$$T(\varpi) = \int_{A_p} (\mathbf{r} \times \sigma(\varpi) \cdot \mathbf{n}) \cdot \mathbf{e}_z dA = 0 \tag{3}$$

where σ is the fluid stress, and $\mathbf{n}$ is the outward unit vector normal to the sphere surface. We computed the torque by integrating the contribution from the shear stress along the surface of the sphere and used an iteration based on Newton's method[20] to reach the torque-free rotation rate with the criterion of $T(\varpi) < 10^{-5}$. To approximate the condition of simple shear flow at infinite separation from the sphere, we imposed the condition $\mathbf{u} = \mathbf{u}^{\infty}$ at a spherical outer boundary with a large radius R that can be determined based on the description in Section 2. The velocity field around a neutrally buoyant sphere in simple shear flow can be obtained by simultaneously solving Eqs. 1 and 2 subject to the boundary conditions discussed above.

The first three terms in an expansion for the fluid velocity field in the inner region near a neutrally buoyant sphere in a linear shearing flow take the form:

$$\mathbf{u} = \mathbf{u}^{(0)} + Re\mathbf{u}^{(1)} + Re^{3/2}\mathbf{u}^{(2)} \tag{4}$$

Here $\mathbf{u}^{(0)}$ is the well-known stresslet velocity field due to a torque-free sphere in Stokes flow:

$$\mathbf{u}^{(0)} = \Gamma \cdot \mathbf{r} - \frac{1}{r^5}\mathrm{E} \cdot \mathbf{r} - \frac{5}{2}\frac{1}{r^5}(\mathbf{r} \cdot \mathbf{E} \cdot \mathbf{r})\mathbf{r}\left(1 - \frac{1}{r^2}\right) \tag{5}$$

where Γ is the transpose of the velocity gradient tensor and $\mathbf{E}$ is the undisturbed rate of strain. For a simple shear flow, the strain rate and velocity gradient tensors are given by

$$\mathbf{E} = \frac{1}{2}[(\nabla \mathbf{u}) + (\nabla \mathbf{u})^{\mathrm{T}}] = \begin{pmatrix} 0 & \frac{1}{2} & 0 \\ \frac{1}{2} & 0 & 0 \\ 0 & 0 & 0 \end{pmatrix} \tag{6}$$

$$\Gamma = (\nabla \mathbf{u})^{\mathrm{T}} = \begin{pmatrix} 0 & 1 & 0 \\ 0 & 0 & 0 \\ 0 & 0 & 0 \end{pmatrix} \tag{7}$$

corresponding to $\mathbf{u}^{\infty} = (y, 0, 0)$. The Stokes flow in a spherical coordinate system (r, θ, ϕ) with the particle center at the origin, the azimuthal angle θ measured relative to the z axis, and ϕ measured between the projection of the position vector into the xy-plane and the x axis is

$$u_r^{(0)} = \frac{1}{r}\mathbf{E} : \mathbf{rr}\left(1 - \frac{5}{2}\frac{1}{r^3} + \frac{3}{2}\frac{1}{r^5}\right) = r\,\sin^2\theta\,\sin\phi\,\cos\phi\left(1 - \frac{5}{2}\frac{1}{r^3} + \frac{3}{2}\frac{1}{r^5}\right) \tag{8}$$

$$u_\theta^{(0)} = \mathbf{I}_\theta \cdot \Gamma \cdot \mathbf{r} - \mathbf{I}_\theta \cdot \mathbf{E} \cdot \mathbf{r}\frac{1}{r^5} = \mathrm{I}_\theta \cdot \mathrm{E} \cdot \mathbf{r}\left(1 - \frac{1}{r^5}\right) = r\,\sin\theta\,\cos\theta\,\sin\phi\,\cos\phi\left(1 - \frac{1}{r^5}\right) \tag{9}$$

$$u_\phi^{(0)} = \mathbf{I}_\phi \cdot \Gamma \cdot \mathbf{r} - \mathbf{I}_\phi \cdot \mathbf{E} \cdot \mathbf{r}\frac{1}{r^5} = -r\,\sin\theta\,\sin^2\phi\,\, - \frac{1}{2r^4}\sin\theta\,(\cos^2\phi - \sin^2\phi) \tag{10}$$

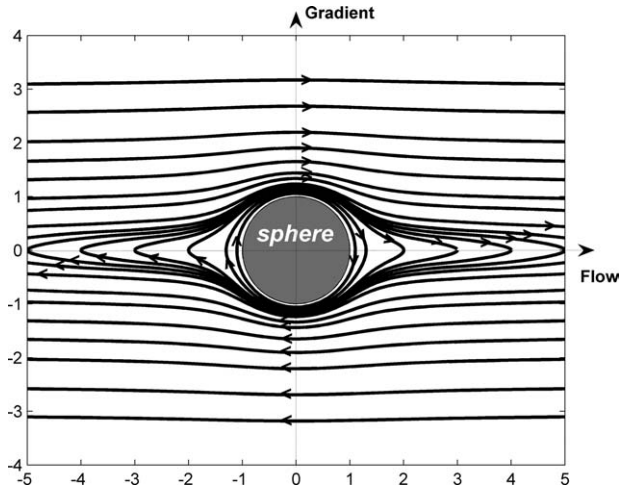

Figure 1. Streamlines in the *xy*-plane for *Re* = 0 from Eqs. 8–10.

In this inertialess limit, streamlines surrounding the torque-free sphere are all closed.

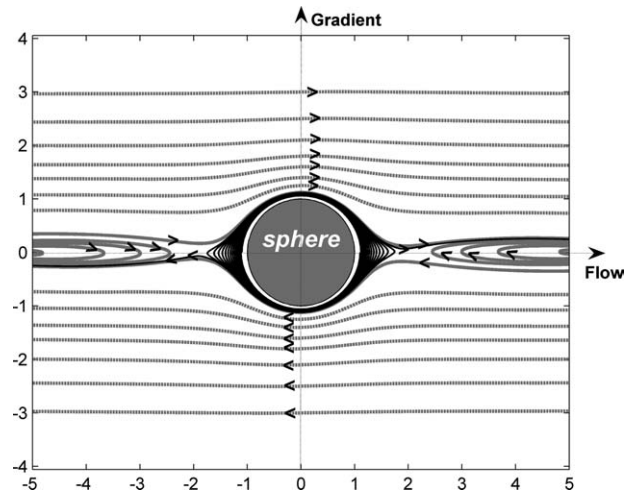

Figure 2. Streamlines in the *xy*-plane for *Re* = 1 in simple shear flow.

The black trajectories depict streamlines that spiral away from the sphere surface and then go downstream, the grey-solid trajectories depict streamlines that pass by the sphere and then form the wakes, and the grey-dot trajectories depict the open streamlines that go from upstream to downstream without spiralling.

The first correction, $\boldsymbol{Re}\mathbf{u}^{(1)}$, to the fluid velocity field near the sphere due to fluid inertia can be determined using a regular perturbation analysis and was first derived by Peery.[14] Subramanian and Koch[1,2] explored the consequences of this correction to the fluid velocity field on the streamline topology and mass transfer at small but non-zero Reynolds numbers. The principal finding of Subramanian and Koch's studies was that centrifugal forces led fluid particles to spiral away from the particle in the flow-gradient plane with the compensatory fluid flux being drawn inward from the vorticity direction. The second correction, $\boldsymbol{Re}^{3/2}\mathbf{u}^{(2)}$, to the fluid velocity field near the particle is required to satisfy the matching condition between the inner and outer fluid velocity solutions. This term contributes to corrections to the particle stresslet and the mass transfer coefficient which we will examine below. The $O(Re^{3/2})$ contribution to the fluid velocity field was first determined by Lin et al.,[21] but this study apparently contained algebraic errors which were corrected by Subramanian et al. (manuscript submitted) in their study of the rheology of emulsions at finite Reynolds numbers. Stone et al. (Personal communication) derived the particle stresslet using a method which employed the generalized reciprocal theorem to avoid an explicit evaluation of the inner velocity field $\boldsymbol{Re}^{3/2}\mathbf{u}^{(2)}$.

Figures 1–3 illustrate the changing topology of the streamlines in the flow-gradient plane with increasing Reynolds number. Figure 1 was produced using the analytical Stokes velocity field of Eqs. 8–10, while Figures 2 and 3 were obtained using our computational solutions for $Re = 1$ and 8. In each case, the streamlines were produced by following the trajectories of non-diffusing fluid phase tracers. It is well known that, as illustrated in Figure 1, a set of closed streamlines surrounds a freely suspended sphere in Stokes flow and that this set of closed streamlines extends to $\pm\infty$ along the x axis. A set of open streamlines exists for sufficiently large values of $|y|$. The streamline pattern for an infinitely long cylinder aligned with the vorticity axis at $Re = 0$ is qualitatively similar.

Robertson and Acrivos[23] solved numerically for the fluid velocity field around a freely suspended cylinder in a simple shear flow at finite Reynolds number. They found that the region of closed streamlines had a finite extent along the x axis. Two symmetrically placed stagnation points appeared along the x axis and for larger values of $|x|$, wakes with reversing fluid trajectories surrounded the x axis. For the two-dimensional finite Reynolds number flow around a

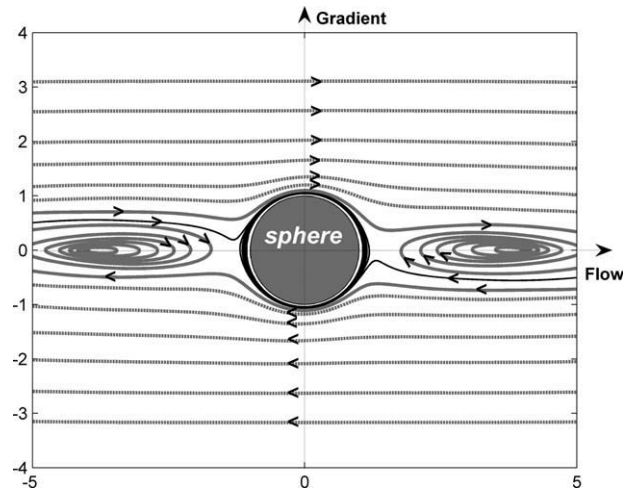

Figure 3. Streamlines in the *xy*-plane for *Re* = 8 in simple shear flow.

The black trajectories depict streamlines that come from the upstream and then spiral towards the sphere surface, the grey-solid trajectories depict streamlines that pass by the sphere and then form the wakes, the grey-dot trajectories depict the open streamlines that go from upstream to downstream without spiraling.

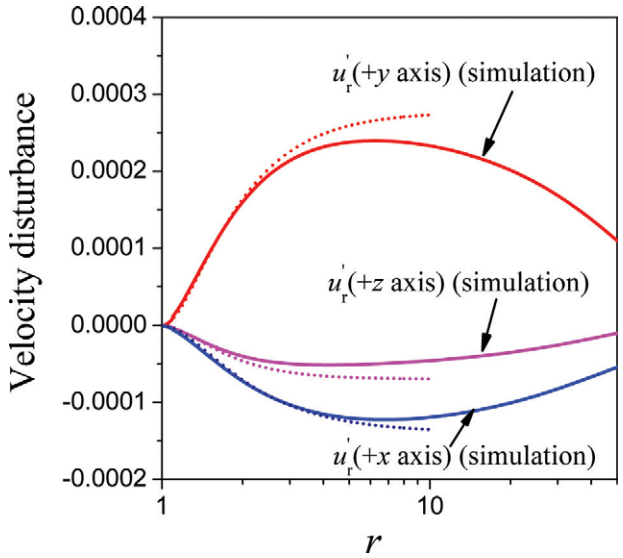

Figure 4. Velocity disturbance in the *r* direction u'_r.

The solid lines, from top to bottom, are u'_r along $+y$, $+z$, and $+x$ axes. The dotted lines are based on the theoretical solutions for the $O(Re)$ disturbance $u_r^{(1)}$. This figure indicates that the finite Re characteristics of the flow, in particular, the incoming flux along x and z axes and the outgoing flux along y axis, are correctly captured by the numerical simulation in the inner region near the particle that controls the mass transfer rate and the Nusselt number. $Re = 0.001$ and the size of computational domain $R/a = 203$. [Color figure can be viewed in the online issue, which is available at wileyonlinelibrary.com.]

cylinder, the antisymmetry of the velocity field about the x axis was preserved and no net inward or outward flux of fluid occurred through any circular surface surrounding the cylinder. Such a flux is prohibited by the incompressible, two-dimensional nature of the flow.

The streamline pattern around a neutrally buoyant particle for a moderately small Reynolds number $Re = 1$ for a freely suspended spherical particle in a simple shear flow is illustrated in Figure 2. As in the case of a cylinder, there are wakes with reversing trajectories (grey-solid trajectories) along the x axis in both the positive and negative directions. However, unlike the case of the cylinder, the streamlines near the particle are not exactly closed orbits. Instead, fluid particles near the sphere spiral outward (black trajectories) and eventually escape along exit channels adjacent to the reversed wakes. At large enough y positions, the trajectories are open. This streamline pattern is qualitatively similar to that obtained by Subramanian and Koch[1,2] using the regular perturbation result for the fluid velocity field, $\mathbf{u} \approx \mathbf{u}^{(0)} + Re\mathbf{u}^{(1)}$ at very small Reynolds numbers. Unlike the case of two-dimensional flow around a cylinder, there is a net flux of fluid through a concentric circle around the sphere in the xy-plane, and this flux is compensated by an inward flux along the vorticity direction. As a result, fluid particles are swept past the sphere by convective motion and a thin mass transfer boundary layer can develop for any non-zero Reynolds number.

Above a critical Reynolds number of about 2.5, we observed that the trajectories of fluid particles spiral toward the sphere in the xy-plane. This behavior is illustrated in Figure 3 for $Re = 8$. In this case, fluid particles in a channel along side the reversing wakes enter the region near the sphere and proceed to spiral toward the sphere (black trajectories). In this case, fluid trajectories approach the sphere along the vorticity axis and within the flow-gradient plane and leave the surface of the sphere at an intermediate angle θ. This point will be discussed further in the context of our boundary layer analysis in next section.

A quantitative comparison of our numerical simulations with the fluid velocity, $\mathbf{u} \approx \mathbf{u}^{(0)} + Re\mathbf{u}^{(1)}$, predicted for the inner region near the sphere, is given in Figure 4, where we plot the radial component of the fluid velocity as a function of radial position along the $+x$, $+y$, and $+z$ axes for $Re = 0.001$. Since $u_r^{(0)} = 0$ along these axes, plotting the radial velocity at a small value of the Reynolds number isolates the regular perturbation $u_r^{(1)}$ to the fluid velocity. It is seen that the computed fluid velocity is in good agreement with the perturbation analysis for r less than about 4. The deviation between the numerical calculation and the perturbation analysis for larger r can be attributed to the fact that one would eventually enter the inertial outer region for $r = O(Re^{-1/2}) \approx 30$.

Figure 5 is a comparison of our computational results for the rotation rate ϖ of the sphere as a function of Re with previous numerical and experimental work. Our results are in good agreement with the previous computational study of Mikulencak and Morris.[20] The experimental measurements of Poe and Acrivos[24] are close to the computational results for $Re \approx 1$ but lie below the computational results for higher Reynolds numbers. In the experiments, the sphere was held in place by a thin wire and it is possible that the torque acting on this wire contributed to this observed deviation. The fluid flow was also found to be unsteady for $Re > 6$ in the experimental study. The transition to unsteady flow is likely to be influenced by the outer boundary conditions.

The hydrodynamic stresslet for a rigid sphere derived by Batchelor[25] is given by

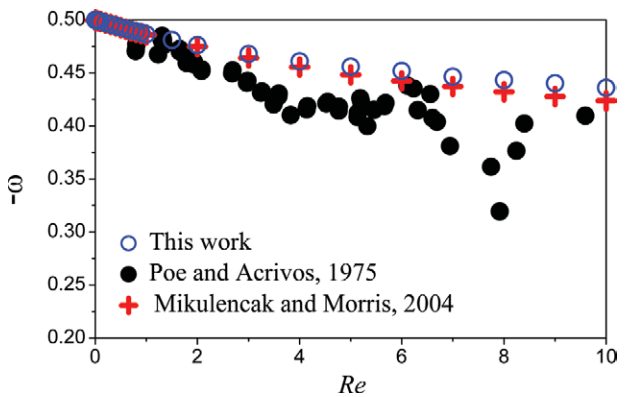

Figure 5. Dimensionless rotation rate of a neutrally buoyant sphere ($\omega = \varpi/\dot{\gamma}$) as a function of Reynolds number.

Our simulations agree with the numerical data of Mikulencak and Morris[20] and the experimental data of Poe and Acrivos.[24] [Color figure can be viewed in the online issue, which is available at wileyonlinelibrary.com.]

$$S_{ij} = \frac{1}{2}\int_{A_p} \left(r_i\sigma_{jk} + r_j\sigma_{ik}\right)n_k \, dA \tag{11}$$

is used to quantify the extra stress occurring within the particle above that which would occur if the constitutive equation of the fluid applied within the particle. The product of S_{ij} with the particle number density represents the particle viscous stress contribution to the mean stress in a dilute suspension. Lin et al.[21] and Stone et al. (Personal communication) have derived the stresslet for a rigid particle including terms up to $O(Re^{3/2})$ in the limit of small Reynolds number. More recently, Subramanian et al. (manuscript submitted) derived the stresslet for an emulsion drop. From this calculation the case of a rigid particle can be obtained in the limit in which the drop viscosity greatly exceeds that of the outer fluid and Subramanian et al.'s result is given by

$$\begin{aligned}\boldsymbol{S} = \frac{\mathbf{10}\pi}{\mathbf{3}}(\mathbf{1_1 1_2} + \mathbf{1_2 1_1}) + \boldsymbol{Re}\Bigg[-\frac{\mathbf{8}\pi}{\mathbf{9}}(\mathbf{1_1 1_1} - \mathbf{1_2 1_2}) \\ + \frac{43\pi}{105}(\mathbf{1_1 1_1} + \mathbf{1_2 1_2})\Bigg] + \frac{50}{9\pi}Re^{\frac{3}{2}}(0.76\mathbf{1_1 1_1} \\ -1.28\mathbf{1_2 1_2} + 1.02(\mathbf{1_1 1_2} + \mathbf{1_2 1_1}) + 0.52\mathbf{1_3 1_3})\end{aligned} \tag{12}$$

where 1, 2, and 3 correspond to the flow, velocity gradient, and vorticity directions of the simple shear flow, respectively. The numerical coefficients in Eq. 12 differ from those derived by Lin et al.[21] and Stone et al. (personal communication), and we believe that these studies suffered from algebraic errors. The stresslet contributions to the shear stress S_{12}, first normal stress difference $S_{11} - S_{22}$, and second normal stress difference $S_{22} - S_{33}$ are plotted as functions of Re in Figure 6. Figures 6a–c give the results for Reynolds numbers as large as 10 and show that the computations are in good agreement with the previous computational study of Mikulencak and Morris.[20] It should also be noted that larger deviations for the shear stress occur at some points in Figure 6a. We have found the fact that the shear stress was more sensitive to the computing domain size than the normal stress differences were (Subramanian et al., submitted), so these deviations might result from the fact that the computing domain size used by Mikulencak and Morris is different from ours. At a very small Reynolds number $Re = 10^{-5}$, our results for the particle rotation rate $\varpi_0 = -0.5000$ and shear stresslet $S_{12,0} = 10.39$ are very close to those $\varpi_0 = -0.5$ and $S_{12,0} = \frac{10}{3}\pi = 10.47$ predicted for Stokes flow. In Figures 6d–f, we plot the components of the stress divided by the Reynolds number, i.e., $-(S_{11} - S_{22})/Re$, $(S_{22} - S_{33})/Re$, and $(S_{12} - S_{12,0})/Re$ versus $Re^{1/2}$ to facilitate comparison with the theories (Subramanian et al., submitted; Stone et al., Personal communication)[21] for small but non-zero Reynolds numbers. These three figures show very good agreement with the theoretical predictions of Subramanian et al. for the normal stresses and fair agreement for the shear stress (manuscript submitted). For example, the slope and intercept of the plot of $-(S_{11} - S_{22})/Re$ against $Re^{1/2}$ obtained from our simulations for $Re \leq 0.1$ are -3.36 and 5.51, respectively, which are very close to the values -3.61 and 5.58 derived by Subramanian et al. (manuscript submitted) and -3.34 and 5.59 derived by Stone et al. (personal communication). The slope -1.20 derived by Lin et al.[21] is about a factor of 3 smaller than our numerical results and the other theories. Similarly, we can obtain a slope of -3.25 and an intercept of 4.14 by fitting our numerical $(S_{22} - S_{33})/Re$ against $Re^{1/2}$ for $Re \leq 0.1$, which are also in good agreement with the analytical predictions namely -3.18 and 4.08 derived by Subramanian and Koch but deviate from the slopes derived the slope value by Lin et al. (-1.06) and Stone et al. (-1.56). As can been seen in Figure 6d, the fitted line for $(S_{12} - S_{12,0})/Re$ versus $Re^{1/2}$ for the same $Re \leq 0.1$ gives a slope of 1.23, which shows a larger difference from the value of 1.8 derived by Subramanian and Koch and Stone et al. The computational results for the shear stresslet also do not follow a straight line over a range of Reynolds numbers $Re^{1/2} < 0.3$ as is observed for the normal stresses. We therefore postulate that one may need to explore still smaller Reynolds numbers to obtain quantitative agreement with the theory for the shear stress. Such a study would be very computationally intensive in view of the need to resolve an ever increasing outer inertial length scale.

Mass Transfer from a Sphere at High Peclet Numbers

Subramanian and Koch[1,2] performed a boundary layer analysis to determine the rate of mass transfer from a neutrally buoyant sphere in a linear shear flow in the dual limits $Re \ll 1$ and $PeRe \gg 1$. In this section, we make use of our numerical solutions of the Navier-Stokes equations for the flow around a particle in simple shear flow to determine the mass transfer coefficient for $Pe \gg 1$ and $Re = 0(1)$. The concentration field for the mass transfer from/to a sphere in a fluid satisfies the dimensionless advection-diffusion equation:

$$Pe(\mathbf{u}\cdot\nabla C) = \nabla^2 C \tag{13}$$

with the boundary conditions:

$$C = 1, \qquad \text{at the surface of particle} \quad r = 1 \tag{14}$$

$$C = 0, \qquad \text{as } r \to \infty \tag{15}$$

where the radial coordinate r is non-dimensionalized by a. For sufficiently large Peclet number ($Pe \gg 1$), the resistance to mass transfer in a boundary layer near the surface of the sphere dominates the rate of mass transfer from the sphere.

Letting $\lambda = r - 1$ so that λ is close to zero in the boundary layer, the fluid velocity components can be expanded as Taylor series:

$$u_r = u_r|_{\lambda=0} + \frac{1}{2}\lambda^2\frac{\partial^2 u_r}{\partial\lambda^2}\bigg|_{\lambda=0} + O(\lambda^3) \tag{16}$$

$$u_\theta = u_\theta|_{\lambda=0} + \lambda\frac{\partial u_\theta}{\partial\lambda}\bigg|_{\lambda=0} + O(\lambda^2) \tag{17}$$

$$u_\phi = u_\phi|_{\lambda=0} + \lambda\frac{\partial u_\phi}{\partial\lambda}\bigg|_{\lambda=0} + O(\lambda^2) \tag{18}$$

where $u_\theta|_{\lambda=0} = 0$ and $u_r|_{\lambda=0} = 0$ at the surface of the sphere.

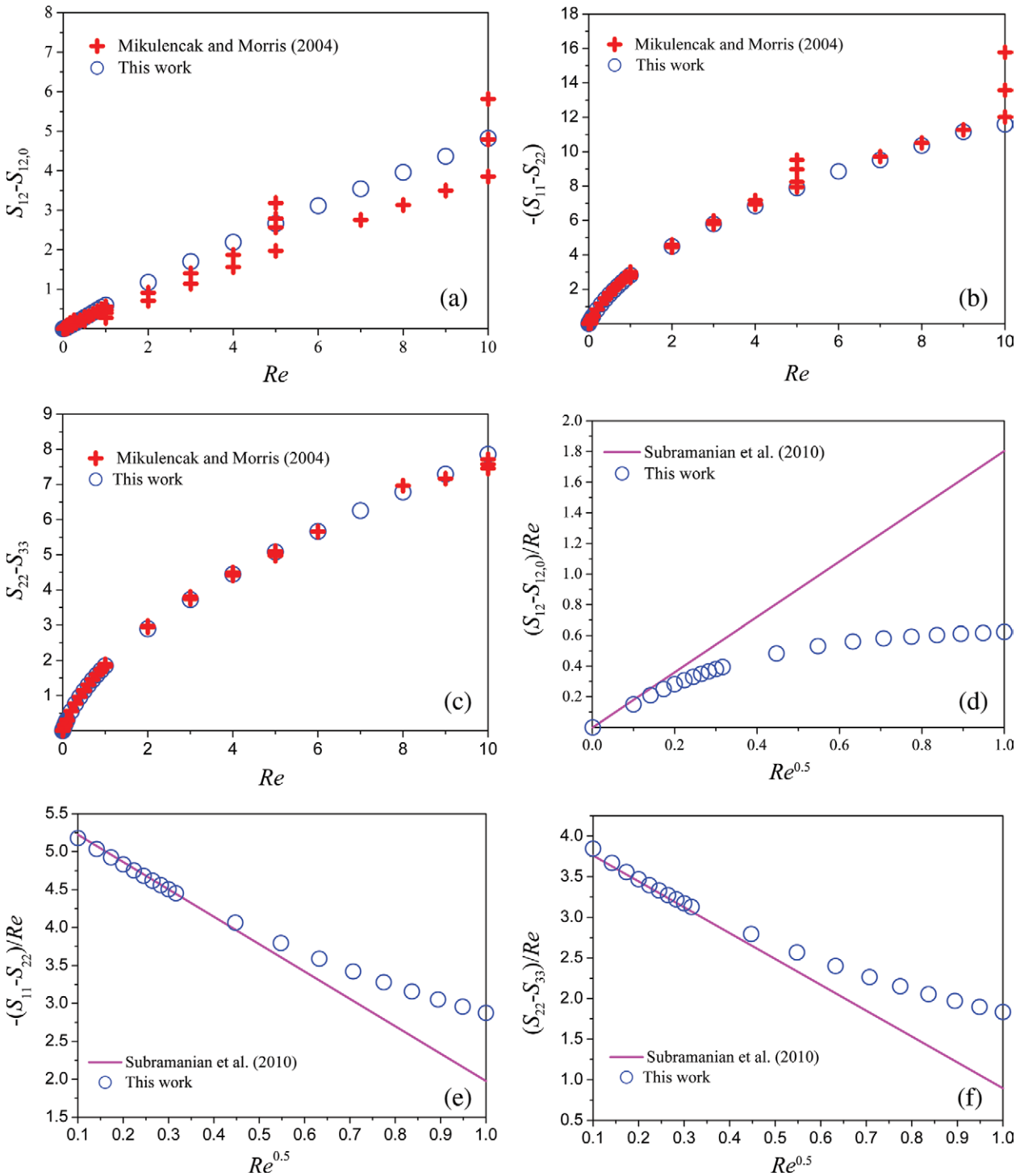

Figure 6. The stresslet S_{ij} as a function of Reynolds number.

(a) Shear component of the stresslet S_{12} less the Stokes contribution $S_{12,0}$; (b) negative of first normal stress difference $-(S_{11}-S_{22})$; (c) second normal stress difference $S_{22}-S_{33}$; (d) $(S_{12}-S_{12,0})/Re$ as a function of $Re^{1/2}$; (e) $-(S_{11}-S_{22})/Re$ as a function of $Re^{1/2}$; (f) $(S_{22}-S_{33})/Re$ as a function of $Re^{1/2}$. Our data agree with Mikulencak and Morris[20] well and are in good agreement with the theoretical predictions by Subramanian et al. (manuscript submitted) for $Re < 0.1$. [Color figure can be viewed in the online issue, which is available at wileyonlinelibrary.com.]

Since the λ is of the order of the boundary layer thickness at large Pe, the radial and tangential velocities are asymptotically smaller when compared to the azimuthal component, i.e., $u_r \ll u_\phi$ and $u_\theta \ll u_\phi$. So at leading order Eq. 13 can be simplified to

$$\frac{\partial C}{\partial \phi} = 0 \tag{19}$$

To a first approximation, the azimuthal dependence of the concentration field may be neglected near the sphere surface. We have

$$C(r,\theta,\phi) = C^{(0)}(r,\theta) + f(Pe)C^{(1)}(r,\theta,\phi) \tag{20}$$

and $f(Pe) \ll 1$. Equation 13 is therefore written as

$$\frac{1}{2}\lambda^2\left(\frac{\partial^2 u_r}{\partial \lambda^2}\bigg|_{\lambda=0}\right)\frac{\partial C^{(0)}}{\partial r} + \frac{1}{r}\lambda\left(\frac{\partial u_\theta}{\partial \lambda}\bigg|_{\lambda=0}\right)\frac{\partial C^{(0)}}{\partial \theta} + f(Pe)\frac{1}{r\sin\theta}\lambda\left(\frac{\partial u_\phi}{\partial \lambda}\bigg|_{\lambda=0}\right)\frac{\partial C^{(1)}}{\partial \phi} = \frac{1}{Pe}\nabla^2 C^{(0)} \tag{21}$$

An equation for the leading order concentration field $C^{(0)}$, which is independent of ϕ can be obtained by integrating the mass conservation Eq. 21 over the azimuthal coordinate $\phi = (0, 2\pi)$ to obtain

$$\eta^2 \bar{h}_1(\theta)\frac{\partial C^{(0)}}{\partial \eta} + \eta \bar{h}_2(\theta)\frac{\partial C^{(0)}}{\partial \theta} = \frac{\partial^2 C^{(0)}}{\partial \eta^2} \tag{22}$$

where $\eta = \lambda\, Pe^{1/3}$,

$$\bar{h}_1(\theta) = \frac{1}{2\pi}\int_0^{2\pi}\left(\frac{1}{2}\frac{\partial^2 u_r}{\partial \lambda^2}\bigg|_{\lambda=0}\right)d\phi \tag{23}$$

is the azimuthal average of half the second derivative of the radial velocity and

$$\bar{h}_2(\theta) = \frac{1}{2\pi}\int_0^{2\pi}\left(\frac{\partial u_\theta}{\partial \lambda}\bigg|_{\lambda=0}\right)d\phi \tag{24}$$

is the azimuthal average of the surface gradient of u_θ. From continuity, we find

$$\bar{h}_1(\theta) = -\frac{1}{2}\frac{1}{\sin\theta}\frac{d}{d\theta}(\bar{h}_2(\theta)\sin\theta) \tag{25}$$

The leading order fluid velocity near the sphere is a solid body rotation. However, this motion yields no net transport of mass across the boundary layer. Upon averaging over ϕ, the convective velocity in the mass conservation Eq. 22 consists of radial inward and outward flows and a shearing flow in the θ direction that sweeps the fluid across the boundary layer. The value of the azimuthal average of $\partial u_\theta/\partial r$, i.e., $\bar{h}_2(\theta)$ defined in Eq. 24, indicates the direction of the fluid flux along the sphere. A positive value of $\bar{h}_2(\theta)$ indicates that fluid in the boundary layer is being convected from the z axis toward the xy-plane, whereas a negative value of $\bar{h}_2(\theta)$ indicates that fluid is being convected toward the z axis. As illustrated in Figure 7, $\bar{h}_2(\theta)$ is positive for all $0 \le \theta \le \pi/2$ for $Re = 0.1$ and 1 indicating that fluid is convected from the vorticity axis to the flow gradient plane and a wake forms as fluid is convected away from the sphere at the

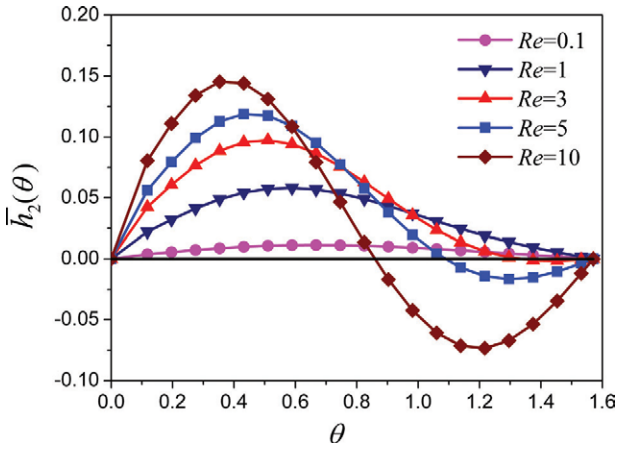

Figure 7. Azimuthally (ϕ) averaged $\partial u_\theta/\partial r$ near the sphere surface namely $\bar{h}_2(\theta)$ defined in Eq. 24 as a function of polar angle (θ) for different Reynolds numbers.

$\bar{h}_2(\theta)$ is always larger than zero at $Re = 0.1$ and 1, but negative value appears near $\theta = \pi/2$ when Re reaches 3. The range of θ at which $\bar{h}_2(\theta)$ is negative enlarges with increasing Re as shown by the results at $Re = 5$ and $Re = 10$. [Color figure can be viewed in the online issue, which is available at wileyonlinelibrary.com.]

flow-gradient plane. We find that this trend occurs up to a critical Reynolds number of about 2.5. At higher Reynolds numbers, the sign of $\bar{h}_2(\theta)$ changes at an intermediate angle between $\theta = 0$ and $\theta = \pi/2$. At these higher Reynolds numbers, fluid moves toward the sphere at the vorticity axis and at the flow-gradient plane and migrates toward the intermediate angle, where $\bar{h}_2(\theta)$ changes sign and it is at this angle that a wake forms. The angle at which the wake appears decreases with increasing Reynolds number.

Following a procedure similar to that in previous works,[1,2,4] the advection-diffusion equation can be transformed to

$$\frac{d^2 C^{(0)}}{ds^2} + 3s^2\frac{dC^{(0)}}{ds} = 0 \tag{26}$$

$$\bar{h}_1 g^3 + \bar{h}_2 g^2\left(1-\xi^2\right)^{0.5}\frac{dg}{d\xi} = -3 \tag{27}$$

where $s = \eta/g(\xi)$ is a rescaled radial coordinate, g is the scaled boundary layer thickness, and $\xi = \cos\theta$. The solution of Eq. 26 that satisfies the concentration boundary conditions on the sphere and at large radial distances from the sphere is

$$C^{(0)}(s) = \frac{1}{\Gamma\left(\frac{4}{3}\right)}\int_s^\infty e^{-s'^3}ds' \tag{28}$$

The Eq. 27 for the boundary layer thickness must be integrated in the negative ξ direction when $\bar{h}_2(\theta) > 0$ and in the positive ξ direction when $\bar{h}_2(\theta) < 0$. Applying the condition that the boundary layer thickness is finite at the point $\theta = 0$ for $\bar{h}_2(\theta) > 0$ and $\theta = \pi/2$ for $\bar{h}_2(\theta) < 0$, we obtain

$$g(\xi)=\frac{9^{\frac{1}{3}}}{(\bar{h}_2(\xi)\sin\theta)^{0.5}}\left(\int_{\xi}^{1}(\bar{h}_2(t)\sin\theta)^{0.5}dt\right)^{\frac{1}{3}} \quad \text{for } \bar{h}_2(t)>0$$

$$g(\xi)=\frac{9^{\frac{1}{3}}}{(-\bar{h}_2(\xi)\sin\theta)^{0.5}}\left(\int_{0}^{\xi}(-\bar{h}_2(t)\sin\theta)^{0.5}dt\right)^{\frac{1}{3}} \quad \text{for } \bar{h}_2(t)<0 \tag{29}$$

Thus, the dimensionless mass transfer rate is finally given by

$$Nu=\frac{1}{4\pi}\int_{\theta=0}^{\theta=\pi}\int_{\phi=0}^{\phi=2\pi}\left(-\frac{\partial C}{\partial \lambda}\bigg|_{\lambda=0}\right)r^2\sin\theta\,d\theta\,d\phi$$
$$=Pe^{\frac{1}{3}}\frac{1}{\Gamma(\frac{4}{3})}\int_0^1\frac{1}{g(\xi)}d\xi \tag{30}$$

where Γ is the gamma function.

In the previous studies,[1,2] Subramanian and Koch used the analytical solution of Peery[14] for $\mathbf{u}^{(1)}$ and that of Lin et al.[21] for $\mathbf{u}^{(2)}$ to determine $\bar{h}_2(\theta)$ in Eq. 24 in the limit of small Reynolds number and thereby derive the mass transfer coefficient as $Nu=(0.325-0.0414Re^{1/2})(Re\mathrm{Pe})^{1/3}+O(1)$. More recently, Subramanian et al. (manuscript submitted) found algebraic errors in Lin et al's determination of $\mathbf{u}^{(2)}$ leading to the conclusion that $\bar{h}_2(\theta)$ has the same functional form of θ as that given by Lin et al but with a numerical coefficient that is a factor of 3.04 larger. Using this new prediction for $\bar{h}_2(\theta)$ yields the prediction $Nu=(0.325-0.126\,Re^{1/2})\,(Re\,\mathrm{Pe})^{1/3}+O(1)$ for $Re\ll 1$ and $Pe\ Re\gg 1$. In the present study, we have to use the numerical solution for the velocity at finite Reynolds number to calculate $\bar{h}_2(\theta)$, $g(\xi)$, and Nu by numerical integration. The resulting Nusselt number as a function of Re for simple shear flow is shown in Figure 8. Figure 8a is a linear-linear plot of $Nu/Pe^{1/3}$ versus Re that emphasizes the behavior of the mass transfer coefficient at finite Reynolds numbers. Figure 8b is a plot of $Nu/(RePe)^{1/3}$ as a function of $Re^{1/2}$, a form which facilitates comparison with the low Reynolds number analysis since the analytical prediction is a straight line on this graph. The present finite Reynolds number boundary layer analysis is in good agreement with the low Reynolds number analysis for $Re<1$. At higher Reynolds numbers, the finite Reynolds number theory diverges from the small Reynolds number analysis and yields a Nusselt number that continues to grow gradually with increasing Reynolds number.

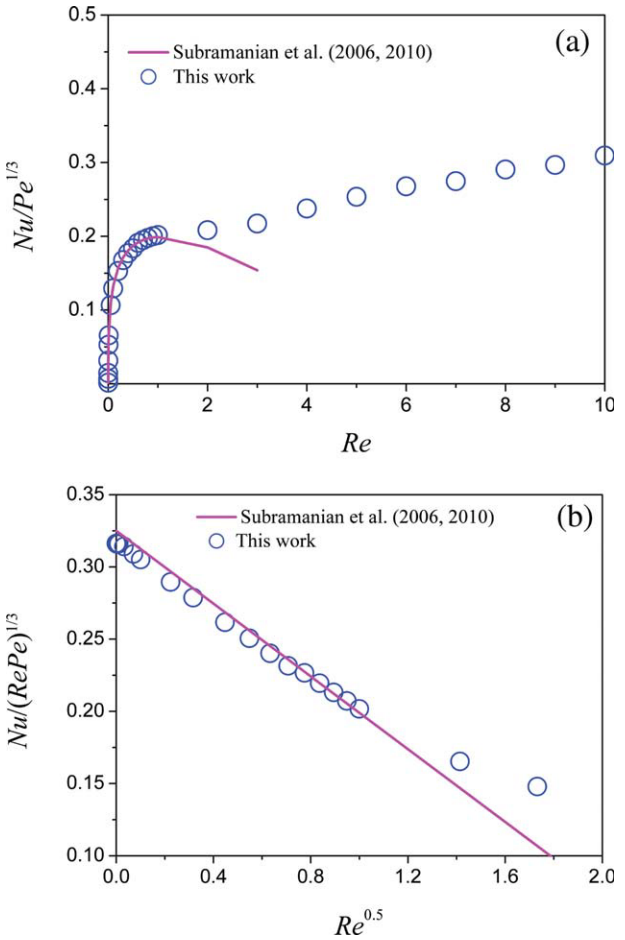

Figure 8. Scaled Nusselt number $Nu/Pe^{1/3}$ as a function of Re (a) and $Nu/(Re\,Pe)^{1/3}$ as a function of $Re^{1/2}$ (b).

Our simulation data agree well with the theoretical predictions of Subramanian and Koch until Re reaches about 1. The fit line of $Nu/(RePe)^{1/3}$ against $Re^{1/2}$ with our simulation data for $Re\le 0.5$ gives a slope of -0.122 and an intercept of 0.317, which are quite close to the theoretical predictions of -0.126 and 0.325. [Color figure can be viewed in the online issue, which is available at wileyonlinelibrary.com.]

Mass Transfer from a Sphere at Finite *Pe*

As we cannot obtain an analytical prediction for the mass/heat transfer rates at finite Peclet numbers, numerical simulations of the mass transfer from a neutrally buoyant sphere in simple shear flow is presented in this section. The unsteady mass transfer at finite Pe is governed by the general advection-diffusion equation:

$$\frac{\partial C}{\partial t}+Pe\,(\mathbf{u}\cdot\nabla C)\;=\nabla^2 C \tag{31}$$

with the same boundary conditions as in Eqs. 14 and 15, where t is the dimensionless mass transfer time.

The present code described in Section 2 is verified additionally for the mass transfer from a freely rotating neutrally buoyant sphere with zero sphere velocity in simple shear flow and particle Reynolds number Re approximately zero. Acrivos[3] derived the analytical asymptotic Nu for simple shear flow past a sphere at infinite Pe and zero Re, i.e., $Nu\approx 4.5$. The Nusselt number approaches a finite value in the limit of high Peclet number in this case, because the chemical tracer must diffuse across the region of closed streamlines seen in Figure 1a. Because of the recirculating streamlines, there is no thin boundary layer formed in this limit. To calculate the mass transfer at $Re=0$, we can either use the analytical velocity (Eqs. 8–10) or compute the fluid velocities in (r, θ, ϕ) by setting the shear rate close to zero or specifying the viscosity of the fluid as being large enough to make Re very small. Computational results for the Nusselt number determined using the analytical velocity field are presented as a function of Peclet number in Figure 9a for

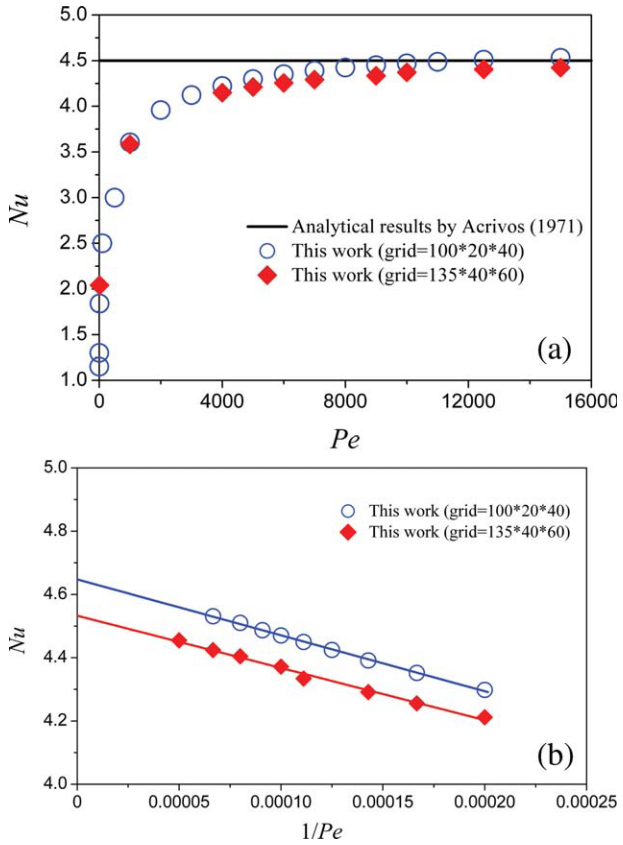

Figure 9. Nusselt number representing mass transfer from a neutrally buoyant sphere in simple shear flow as a function of Peclet number.

The flow field is based on the analytical solution (Eqs. 8–10) for Stokes flow ($Re = 0$). Comparison between the results obtained using different grids of $100(r) \times 20(\theta) \times 40(\phi)$ with $\Delta r = 0.005a$ near the surface and $135(r) \times 40(\theta) \times 60(\phi)$ with $\Delta r = 0.00125a$ near the surface shows the effect of grid resolution. [Color figure can be viewed in the online issue, which is available at wileyonlinelibrary.com.]

two computational grids, a coarser grid with $100(r) \times 20(\theta) \times 40(\phi)$ and a finer grid with $135(r) \times 40(\theta) \times 60(\phi)$. It can be seen that the Nusselt number rises rapidly from the value 1 for pure diffusion and reaches a value of about 4 at a Peclet number of about 2000. Thereafter, the Nusselt number rises more slowly and appears to approach a value close to the theoretical prediction of 4.5 when $Pe \approx 10{,}000$.

The analysis of Acrivos[3] indicates that, to leading order for large Peclet number, the concentration field is a constant along each of the closed streamlines. The values of these constants are determined based on a balance of the diffusive flux acting perpendicular to the streamlines. One might expect that the first correction to the concentration field determined by Acrivos would be a regular perturbation giving the effects of diffusion parallel to the streamlines. This would yield an $O(1/Pe)$ correction to the concentration field and thereby the Nusselt number. On this basis, we might expect the relationship between Nusselt number and Peclet number at $Re = 0$ to take the form $\boldsymbol{Nu = k_0 + k_1/Pe}$. Figure 9b shows that this form gives a good fit to the numerical simulation data for $Pe > 5000$. The intercept k_0 obtained in this way is 4.65 for the coarser and 4.53 for the finer grid. This indicates that the computation of the concentration field is well resolved and is in good agreement with Acrivos' analytical prediction $Nu = 4.5$ as $Pe \to \infty$.

The good agreement with Acrivos' theory confirms the accuracy of our numerical method, and we now turn to apply this method to determine the rate of mass transfer from a neutrally buoyant sphere in simple shear flow at finite Reynolds and Peclet numbers. We will examine the dependence of the Nusselt number on Pe and Re, plot contours of the concentration field, and examine aspects of the concentration field near the particle that elucidate the comparison of the finite Peclet number mass transfer to the $Pe \gg 1$ boundary layer theory.

As shown in Figure 10, the numerical Nusselt number for the mass transfer at the finite value $Re = 0.3$ increases monotonically with increasing Peclet number. For a Peclet number of 10,000, the Nusselt number already exceeds the value 4.5 predicted for $Re = 0$ and $Pe \to \infty$. This confirms Subramanian and Koch's[1,2] assertion that breaking of the symmetry of the streamlines by fluid inertia enhances mass transfer. The effect of grid resolution may also be observed from Figure 10: the numerical results obtained with a coarser grid of $80(r) \times 20(\theta) \times 40(\phi)$ and a finer grid of $106(r) \times 40(\theta) \times 60(\phi)$ agree with each other for Pe up to 20,000, with relative errors less than 5.5%. However, the difference becomes significant when Pe exceeds 20,000. This suggests that the two grids used in our study are sufficient only for $Pe < 20{,}000$. It would be ideal to use a more refined grid to solve the mass transfer at even higher Peclet numbers. However, due to the much longer computing time required, we limited ourselves to cases with Pe less than 20,000 in this study.

The Nusselt number for mass/heat transport is often correlated with the Schmidt number $Sc = Pe/Re = \nu/D$, since this dimensionless number remains constant in a series of experiments using the same fluid-tracer system.[4] Figure 11 is a plot of the Nusselt number versus Reynolds number for two finite values of the Schmidt number ($Sc = 300$ and 10,000). The Nusselt number grows rapidly with increasing Reynolds number and grows fastest at the larger value of Sc

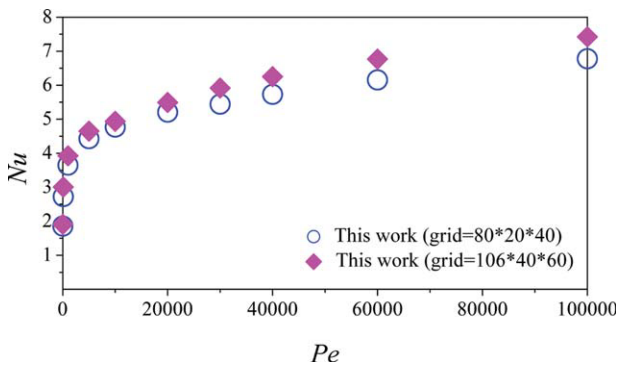

Figure 10. Scaled Nusselt number *Nu* as a function of *Pe* for *Re* = 0.3.

Comparison between results obtained using different grids of $80(r) \times 20(\theta) \times 40(\phi)$ with $\Delta r = 0.01a$ near the surface and $106(r) \times 40(\theta) \times 60(\phi)$ with $\Delta r = 0.0025a$ near the surface shows the effect of grid resolution. [Color figure can be viewed in the online issue, which is available at wileyonlinelibrary.com.]

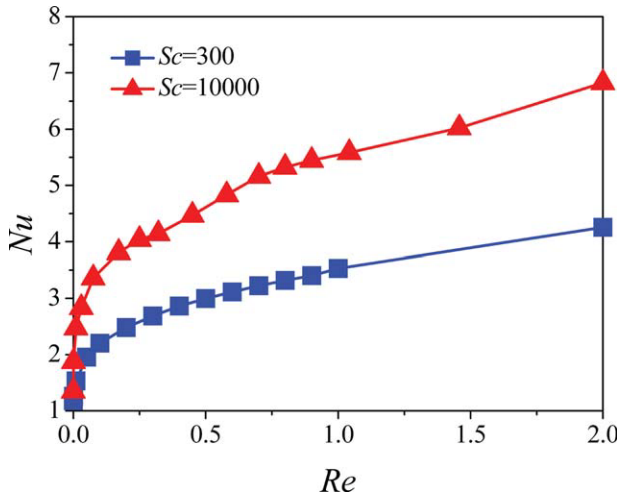

Figure 11. Nusselt number *Nu* as a function of Reynolds number *Re* and Schmidt number *Sc* for a neutrally buoyant, force- and torque-free sphere embedded in a simple shear flow.

[Color figure can be viewed in the online issue, which is available at wileyonlinelibrary.com.]

since in this case the Peclet number is larger for a given value of Re.

At $Sc = \infty$, i.e., very small Re such as in Figure 9, Acrivos[3] showed that the Nusselt number for a small sphere freely rotating in simple shear flow grows from 1.0 at $Pe = 0$ and then approaches a constant of about 4.5 as $Pe \to \infty$. Thus, it would be interesting to look at Nu as a function of Pe at fixed finite Sc. As shown in Figure 12, the Nusselt number at finite Sc does not approach a constant as $Pe \to \infty$ but rather continues to grow without bound. The curves for different Schmidt numbers coincide with one another if the Reynolds number is smaller than about 0.1 (corresponding to $Pe = 30$ in the case of $Sc = 300$). At larger Pe and Re, the curves diverge and it can be seen that around $Re = 1$ (marked by the + sign) the Nusselt number begins to grow rapidly with increasing Peclet number. These observations are consistent with Subramanian and Koch's[1,2] mechanism of enhanced mass transfer due to inertially induced changes in streamline topology.

Figure 13 shows concentration profiles around a neutrally buoyant sphere in simple shear flow at different Schmidt numbers and Re (or Pe). From these figures, one can observe that the distortion of the concentration contour lines develops gradually with increasing Re to form a series of closed contours. As shown in Figures 1–3, the patterns of streamlines become more complicated with increasing Reynolds number, with spiraling streamlines and formation of stagnation points. Figure 13a is a plot of the concentration profiles for $Re = 0$ and $Pe = 9000$. The isoconcentration surfaces in this case have a similar shape to the closed streamlines in Figure 1, confirming the central premise of Acrivos'[3] asymptotic analysis that the concentration is nearly constant along a closed streamline at high Peclet number. The isoconcentration surfaces in Figures 13b, c at $Re = 0.01$ and $Re = 1$ show that inertia breaks the symmetry of the concentration field just as it breaks the symmetry of the velocity field in Figure 2. As compared in Figures 13c–e at fixed $Re = 1$, with increasing Schmidt numbers, the concentration contour lines become more and more distorted and concentration wakes extend away from the sphere in $+x$ and $-x$ directions, as the mass transfer process is gradually dominated by convection with increasing Pe. The larger the value of Re, Pe, or Sc, the more severely distorted the concentration contours. The mass comes from the neutrally buoyant sphere in simple shear flow and spirals out a certain distance and then escapes in one of the channels where it can be convected downstream. As shown in Figures 13c, d, the reverse wake on the right side of the particle is tilted downward, and the higher concentration contours on the right are tilted upward. This suggests that the mass is being convected into channels that lie in the extensional quadrant above the reverse wake as suggested by Subramanian and Koch.[2]

In the previous section, we presented a boundary layer theory for mass transfer for $Pe \gg 1$ and finite Re. We showed that this theory was consistent with the previous work of Subramanian et al. (manuscript submitted)[1,2] for $Re \ll 1$. We will now examine some of the assumptions that underlie the theory using results from the numerical simulations examining the behavior for $Re = 0.3$. The boundary layer theory indicates that the variation of the concentration in the boundary layer is approximately independent of ϕ at a given value of θ. In Figure 14a, we plot the concentration gradient dc/dr at the particle surface as a function of ϕ for $\theta = 0.67$. It is seen that the variation of dc/dr with respect to ϕ becomes weaker as the Peclet number is increased from 5000 to 10,000 and 20,000 and is negligible for $Pe >$ 10,000. This justifies the use of the ϕ-averaged mass conservation equation and the ϕ-averaged concentration field. In Figure 14b, we compare the ϕ-averaged concentration gradient at the surface scaled with the boundary layer thickness, i.e., $(-dc/dr)/Pe^{1/3}$ for $Pe = 5000$, 10,000, and 20,000

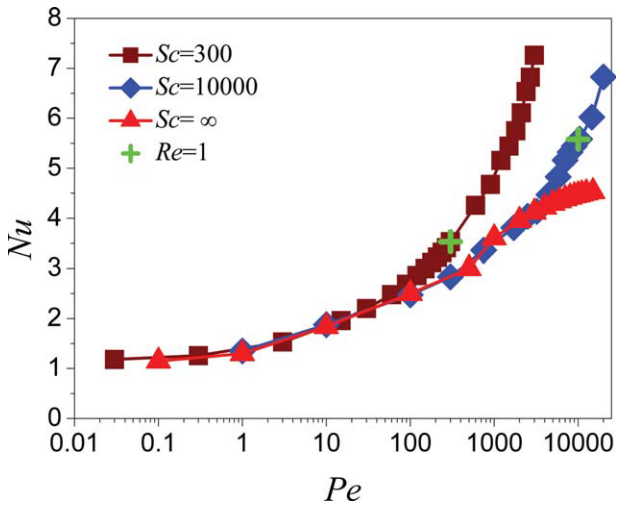

Figure 12. Nusselt number *Nu* as a function of Peclet number *Pe* and Schmidt number *Sc* for a neutrally buoyant, force- and torque-free sphere embedded in a simple shear flow.

[Color figure can be viewed in the online issue, which is available at wileyonlinelibrary.com.]

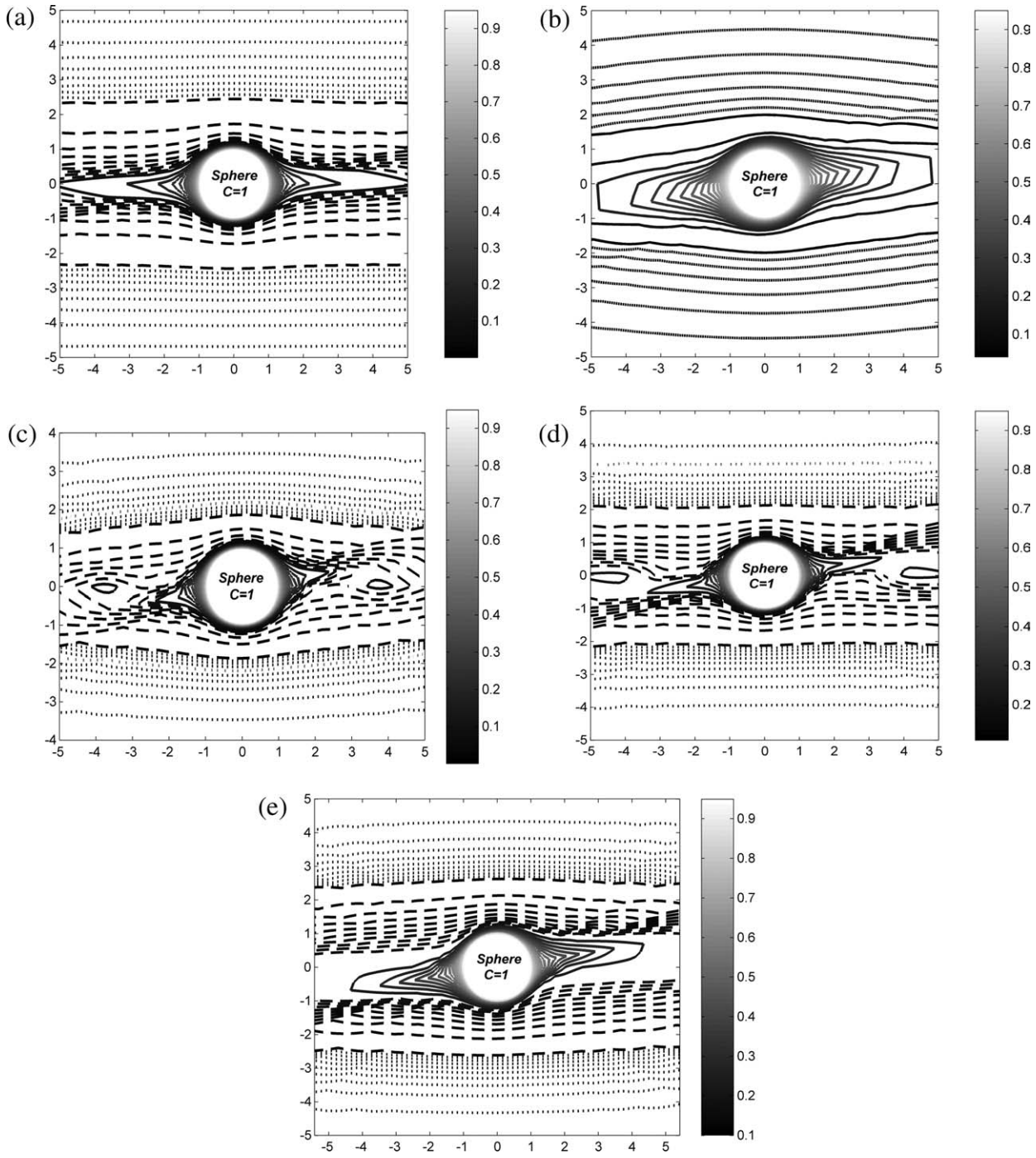

Figure 13. Contour of solute concentration (*C*) obtained using a grid of $75(\mathbf{r})\times40(\theta)\times40(\phi)$ with $\Delta r = 0.005a$ around a neutrally buoyant, force- and torque-free sphere embedded in a simple shear flow: (a) *Re* = 0, *Pe* = 9000; (b) *Re* = 0.01, *Pe* = 100, yielding *Sc* = 10,000; (c) *Re* = 1, *Pe* = 10,000, yielding *Sc* = 10,000; (d) *Re* = 1, *Pe* = 3000, yielding *Sc* = 3000; (e) *Re* = 1, *Pe* = 300, yielding *Sc* = 300.

In these figures, different types of lines are used to describe the variation of concentration in the radial direction: the difference of dimensionless concentration between two adjacent solid, dashed and dotted lines is 0.05, 0.01, and 0.001, respectively. These figures show as *Re* increases, the concentration contours become more and more distorted, and increasing *Pe*, on the other hand, increases the concentration gradient and decreases the thickness of the mass transfer boundary layer.

with the boundary layer predictions for $Pe \gg 1$, i.e., $1/\Gamma(\frac{4}{3})/g(\xi)$. The numerical simulation results are in good agreement with the boundary layer theory for $\theta < 0.7$, 0.9, and 1.1 at $Pe = 5000$, 10,000, and 20,000. With regard to the deviation for the first point at very small θ, it is likely due to the limited numerical accuracy of $g(\xi)$ at small θ. Considering the calculating formula of $\overline{h}_2(\xi)$ namely Eq. 24, the value of $\overline{h}_2(\xi)$ would approach zero when θ tends toward

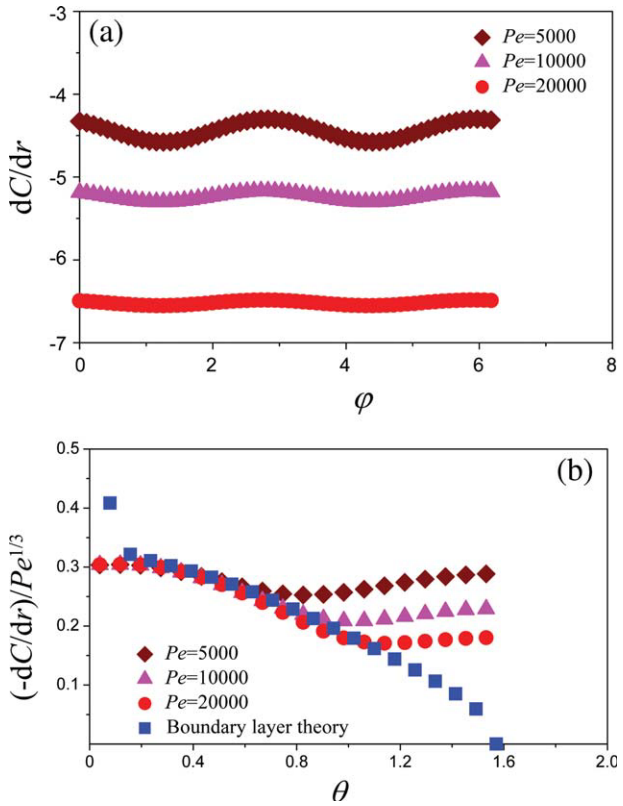

Figure 14. Variation of the concentration gradient *dc/dr* on sphere surface in the azimuthal (ϕ) direction at a fixed polar angle $\theta = 0.67$ (a) and variation of the azimuthally averaged concentration gradient $(-dC/dr)/Pe^{1/3}$ on the sphere surface in the polar (θ) directions (b) for the case of *Re* = 0.3.

[Color figure can be viewed in the online issue, which is available at wileyonlinelibrary.com.]

zero since $\partial u_\theta/\partial \lambda$ is indeed zero at z axis ($\theta = 0$). When we calculated the value of $g(\xi)$ at the grid node closest to $\theta = 0$, however, we had to do an interpolation between two very small values of $\overline{h}_2(\xi)$ at this node and an adjacent node to get a numerical approximation of the integral in Eq. 29, which led to a greater numerical error than elsewhere. In principle, increasing the number of grid nodes should reduce the numerical error; however to keep the computational time reasonable, we chose not to increase it any further. At angular positions closer to the flow-gradient plane, the finite *Pe* concentration gradient levels off, while the boundary layer theory predicts an ever decreasing concentration gradient. It is expected that a wake will form near the flow-gradient plane in which angular diffusion, which is neglected in the boundary layer analysis, becomes important. The angular extent of this wake should become asymptotically small as $Pe \rightarrow \infty$. The wake seen in the numerical simulations is indeed becoming smaller with increasing Peclet number, but apparently a Peclet number of 20,000 is not yet large enough to make the portion of the sphere covered by the wake negligible. Thus, although the Nusselt number at finite *Re* is seen to grow indefinitely with increasing *Pe* in qualitative agreement with the boundary layer prediction, $Pe = 20{,}000$ is not sufficiently large to obtain quantitative agreement between the asymptotic theory and the numerical simulations.

Conclusions

The flow field and mass transfer from a neutrally buoyant sphere in simple shear flow are numerically simulated in this work. We extend Subramanian and Koch's boundary layer analysis for $Re \ll 1$ and $Pe\ Re \gg 1$ to $Re = O(1)$ and finite Peclet number. A finite difference method with the control volume formulation and SIMPLE algorithm is adopted to solve the shear flow at finite Reynolds numbers. A fifth-order WENO scheme in spatial discretization and a third-order TVD Runge–Kutta scheme in time are applied for the solution of the advective-diffusion mass transport equation.

The predicted rotation rate of the sphere and the hydrodynamic stresslet agree with the simulated results by Mikulencak and Morris at finite *Re* and the analytical predictions at small *Re*. At zero Reynolds number, a set of closed streamlines envelops the particle. At small, finite Reynolds numbers, we find that the streamlines in the flow-gradient plane spiral away from the particle as predicted by Subramanian and Koch.[1,2] However, above a critical Reynolds number of about 2.5, streamlines in the flow gradient plane spiral toward the particle. At these larger Reynolds number, the fluid flux in the boundary layer adjacent to the particle goes from the flow-gradient plane and from the vorticity axis toward an intermediate angular position where the fluid moves away from the sphere forming a wake.

A boundary layer analysis coupled with numerical simulation is used to compute the mass transfer from a neutrally buoyant sphere at sufficiently large *Pe* and $Re = O(1)$. For $Re \leq 1$, the numerical results agree very well with $Nu = (0.325 - 0.126\,Re^{1/2})\,(Re\,Pe)^{1/3} + O(1)$ derived by Subramanian and Koch at $Re \ll 1$ and $Pe\ Re \gg 1$. At $Re > 1$, the predicted Nusselt numbers begin to deviate from the low Reynolds number theory. It is found that *Nu* continues to increase with increasing Reynolds number up to $Re = 10$, the maximum *Re* studied in this work.

We also obtained the Nusselt numbers for mass transfer from a neutrally buoyant sphere at finite *Pe* and finite *Re* using direct, finite-difference solution of the flow and advection-diffusion equations. The predicted *Nu* at $Re = 0$ increases with increasing Peclet number eventually approaching an asymptote of about 4.5 in agreement with Acrivos's[3] asymptotic analysis. At finite *Re*, the Nusselt number for the mass/heat transfer continues to increase with increasing Peclet number without approaching a constant value as is expected in view of the convective transport away from the sphere surface due to the broken symmetry of the streamlines. An examination of the dependence of the Nusselt number on the Peclet number for fluids with various Schmidt numbers indicates that the *Nu*(*Pe*) relationship remains independent of *Sc* as long as $Re = Pe/Sc$ is less than about 0.1. As the Reynolds number becomes $O(1)$ or larger, the curves for fluids with larger *Sc* diverge showing a rapid increase of *Nu* with increasing *Re*. These results indicate that fluid inertia leads to enhanced mass transport with a trend that is in qualitative agreement with the predictions of Subramanian and Koch.[2] Simulations with finite *Pe* indicate that a very large Peclet number is required before the

wake near the flow-gradient plane becomes small enough to make the boundary layer predictions for the Nusselt number quantitatively accurate. Resolving the concentration field at these very large Peclet numbers numerically would be very computationally intensive.

In future work, we will extend this simulation and boundary layer analysis to the mass transfer from/to a neutrally buoyant spherical drop in simple shear flow at finite *Pe* and finite *Re*. The effect of natural convection with gravity along the vorticity axis, which might be due to the density difference caused by the concentration difference between the solution in equilibrium with the sphere and the solution at infinity, on the mass/heat transfer rate will also be considered.

Acknowledgments

This work was supported by the Department of Energy Grant No. DE-FG02-03-ER46073 and NSF Grant No. CBET-0730579. The first author is grateful for the financial support from the National Natural Science Foundation of China (20990224, 20676134), the National Science Fund for Distinguished Young Scholars, the National Basic Research Program of China (2010CB630904, 2009CB623406), and the Li-Foundation, USA. The authors thank Jeffrey Morris for providing his simulation data and Ganesh Subramanian for useful discussions of the comparison of our numerical solutions with theoretical analysis.

Literature Cited

1. Subramanian G, Koch DL. Centrifugal forces alter streamline topology and greatly enhance the rate of heat and mass transfer from neutrally buoyant particles to a shear flow. *Phys Rev Lett*. 2006;96: 134503-1–134503-4.
2. Subramanian G, Koch DL. Inertial effects on the transfer of heat or mass from neutrally buoyant spheres in a steady linear velocity field. *Phys Fluids*. 2006;18:073302.
3. Acrivos A. Heat transfer at high Peclet number from a small sphere freely rotating in simple shear field. *J Fluid Mech*. 1971;46:233–240.
4. Leal LG. *Laminar Flow and Convective Transport Processes*. London: Butterworth-Heinemann, 1992.
5. Clift R, Grace JR, Weber ME. *Bubbles, Drops, and Particles*. New York: Academic Press, 1978.
6. Acrivos A, Goddard JD. Asymptotic expansions of laminar forced-convection heat and mass transfer. Part 1. Low speed flows. *J Fluid Mech*. 1965;23:273–291.
7. Michaelides EE. Hydrodynamic force and heat/mass transfer from particles, bubbles, and drops-The Freeman scholar lecture. *ASME J Fluids Eng*. 2003;125:209–238.
8. Blackburn HM. Mass and momentum transport from a sphere in steady and oscillatory flows. *Phys Fluids*. 2002;14:3997–4011.
9. Feng ZG, Michaelides EE. A numerical study on the transient heat transfer from a sphere at high Reynolds and Peclet numbers. *Int J Heat Mass Transf*. 2000;43:219–229.
10. Li WZ, Yan YY, Smith JM. A numerical study of the interfacial transport characteristics outside spheroidal bubbles and solids. *Int J Multiphase Flow*. 2003;29:435–460.
11. Yang C, Mao Z-S. Numerical simulation of interphase mass transfer with the level set approach. *Chem Eng Sci*. 2005;60:2643–2660.
12. Masliyah JH, Epstein N. Numerical study of steady flow past spheroids. *J Fluid Mech*. 1970;44:493–512.
13. Bachelor GK. Mass transfer from a particle suspended in fluid with a steady linear ambient velocity distribution. *J Fluid Mech*. 1979;95: 369–400.
14. Peery JH. Fluid mechanics of rigid and deformable particles in shear flow at low Reynolds numbers. Ph.D. Thesis. Princeton University, 1966.
15. Bagchi P, Balachandar S. Effect of free rotation on the motion of a solid sphere in linear shear flow at moderate Re. *Phys Fluids*. 2002; 14:2719–2737.
16. Salem MB, Oesterle B. A shear flow around a spinning sphere: numerical study at moderate Reynolds numbers. *Int J Multiphase Flow*. 1998;24:563–585.
17. Yang BH, Wang J, Joseph DD, Hu HH, Pan TW, Glowinski R. Migration of a sphere in tube flow. *J Fluid Mech*. 2005;540:109–131.
18. Yu ZS, Phan-Thien N, Tanner RI. Dynamic simulation of sphere motion in a vertical tube. *J Fluid Mech*. 2004;518:61–93.
19. Johnson TA, Patel VC. Flow past a sphere up to a Reynolds number of 300. *J Fluid Mech*. 1999;378:19–70.
20. Mikulencak DR, Morris JF. Stationary shear flow around fixed and free bodies at finite Reynolds number. *J Fluid Mech*. 2004;520:215–242.
21. Lin CJ, Peery JH, Schowalter WR. Simple shear flow round a rigid sphere: inertial effects and suspension rheology. *J Fluid Mech*. 1970;44:1–17.
22. Mao Z-S, Chen JY. Numerical solution of viscous flow past a solid sphere with the control volume formulation. *Chin J Chem Eng*. 1997;5:105–116.
23. Robertson CR, Acrivos A. Low Reynolds number shear flow past a rotating cylinder. Part 1. Momentum transfer. *J Fluid Mech*. 1970; 40:685–704.
24. Poe GG, Acrivos A. Closed streamline flows past rotating single spheres and cylinders: inertia effects. *J Fluid Mech*. 1975;72:605–623.
25. Bachelor GK. The stress system in a suspension of force-free particles. *J Fluid Mech*. 1970;41:545–570.

Manuscript received Mar. 17, 2010, and revision received Jun. 30, 2010.